2013 IEEE 10th International Symposium on Biomedical Imaging:
From Nano to Macro
San Francisco, CA, USA, April 7-11, 2013

LEFT VENTRICLE MOTION CLASSIFICATION IN THE MEDIAL SURFACE SHAPE SPACE

Vahid Taimouri

Harvard Medical School
Computational Radiology Laboratory
Children's Hospital Boston, MA, USA

Jing Hua

Wayne State University
Department of Computer Science
Detroit, MI, USA

ABSTRACT

The wall thickness is known as a valuable measure for the cardiac diagnosis. From the geometric point of view, it can be considered as a function defined on the 2D manifold of the medial surface. This paper presents a novel classification method based on medial representation to diagnose and detect the myopathic regions on the left ventricle. A shape space is proposed and constructed based on the changes of the left ventricle wall thickness, in which two shape descriptors are introduced which show remarkable performance to distinguish normal and abnormal left ventricle deformations. The experimental results show that this method can automatically classify the healthy and myopathic subjects and detect myopathic regions on the left ventricle well.

Index Terms— Medial Surface, Shape Space, Medial Representation, Left Ventricle Diagnosis

1. INTRODUCTION

Hypertrophic Cardiomyopathy (HCM) is a well-known cause of heart failure or sudden cardiac death in children [1], in which a portion of myocardium wall becomes thickened, and the normal alignment of muscle cells is disrupted, which obstructs the outflow of blood from the left ventricle. HCM is usually detected by echocardiogram or Cardiac Magnetic Resonance imaging (CMR), which detect the physical properties of the left ventricle wall [2]. However, navigation through sequential poses of a 3D deformation needs highly experienced cardiologists, which increases subjectivity in the analysis. This urges a deformation analysis method which classifies the 3D heart deformations.

Recent researches ([3][4]) have introduced methods that take into account all morphology of the left ventricle in order to localize myocardial regions showing abnormal contractile behavior based on statistics trained from healthy wall motion. Previous studies have applied the medial model to the right/left ventricle deformations and concluded that the medial model can capture the deformation of the left and right ventricles along with the changes of their wall thickness over time [5]. Further, some researchers propose deformable parametric representations of the boundary-medial relationship, i.e. medial representation, which are deformed to fit the interiors of objects to the model structure ([6][7]).

In the medial representation framework, the LV medial surface (**M**) is a topological disk consisting of some *atoms*. Each atom (**m**) contains the center of an inscribed sphere (**x**), the sphere radius (r), and two or three vectors, called *spokes* ($\mathbf{S}_i$), from the sphere centers to the two or three tangent points on the LV boundary (Fig. 1.a), *i.e.*, $\mathbf{m} = \{\mathbf{x}, r, \mathbf{S}_i\} \in \mathbf{M}$. The atoms can be considered as control points on a continuous medial surface [8]. An *end atom* is an atom with three spokes located on the boundary of the medial surface. To simplify the calculations, we do not consider end atoms in this study, thus $\mathbf{m} \in \left\{\mathbb{R}^3 \times \mathbb{R}^+ \times S^2 \times S^2\right\}$. Let points p and q be two points in a neighborhood on a Riemannian manifold **N**. In general, the Log map of q w.r.t. base point p, i.e. $Log_p(q)$, maps q onto the tangent plane of **N** at point p such that, $d_{\mathbf{N}}(p,q) = \|p - Log_p(q)\|$, where $d_{\mathbf{N}}(p,q)$ is the geodesic distance between p and q. In fact, Log map linearizes the non-linear Riemannian manifold by projecting each point onto a linear tangent plane and preserving the distance between two points. As an special case, the Log map between point $x = (x_1, x_2, x_3,)$ and base point $p = (0, 0, 1)$ on a sphere S^2 is computed as,

$$Log_{\mathbf{p}}(\mathbf{x}) = \left(x_1 \cdot \frac{\theta}{\sin(\theta)}, x_2 \cdot \frac{\theta}{\sin(\theta)}\right), \qquad (1)$$

where $\theta = \arccos(x_3)$ is the spherical distance between the point p and x (Fig. 1.b).

This paper aims at extraction of geometrical properties of myocardium wall from the acquired CT images, classification of the left ventricle wall thickness (WT) of two groups of healthy and myopathic subjects, and localization of the myopathic areas. We utilize the medial representation (m-reps) framework and introduce a non-linear shape space based on two novel shape descriptors which capture the changes of the LV wall thickness, and then measure the geodesic distance between each pair of points on the shape space using a novel log map metric. The major novelty is that the constructed shape space can capture the intrinsic geometrical differences between LV deformations and determine the dis/similarity on a non-linearity space. The extrinsic shape variations between

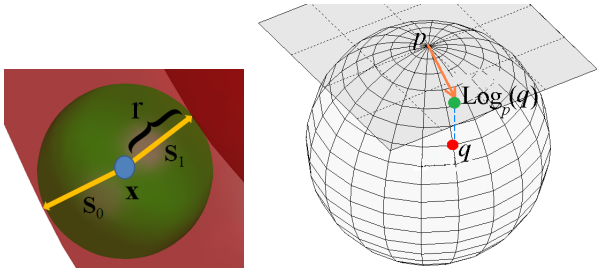

(a) (b)

Fig. 1. (a) A non-boundary atom **m** contains a position (**x**), a radius (r), and two spoke directions ($\mathbf{S}_0$, $\mathbf{S}_1$), (b) The Log map of point q w.r.t. base point p on the sphere S^2.

subjects can be excluded and do not affect the process of classification, which reduces subjectivity in the LV deformation analysis.

2. THE LEFT VENTRICLE MEDIAL SURFACE

Since the myocardium wall becomes thicker in myopathic areas, their corresponding wall thickness changes differently compared with a healthy subject during one heart cycle. Let $r(t_1)$ and $r(t_2)$ be the radius elements of an atom **m** at two sequential time points t_1 and t_2, respectively. The Ratio of Wall Thickness (RWT) at two time points, i.e. $r(t_2)/r(t_1)$, demonstrates the changes of the wall thickness over time. The atoms of the real myopathic regions (delineated by experts) were extracted from the real datasets with HCM, and RWT were calculated at four diastolic and four systolic time points of one heart cycle for atoms in both myopathic and healthy regions.

Our observations reveal that RWT values of atoms in myopathic regions are close to 1 during one heart cycle, which shows these regions cannot contract or expand as the healthy subjects whose RWT values are < 1 in diastole and > 1 in systole. This makes RWT a good candidate to differentiate healthy and myopathic LV's, and localize myopathic regions. However, due to the existence of noise in the acquired images, as well as the lack of accuracy in the extracted medial surface, some atoms in healthy subjects might have RWT values close to one, which lowers the accuracy of RWT as a reliable measure. To tackle this problem, two additional measures are introduced, which can correct and enhance the accuracy of RWT.

2.1. Average of Normal vectors (AoN)

Let $\hat{\mathbf{M}}$ be the set of all atoms whose RWT value is close to one, which are candidates of being in the myopathic region, and let **n** be normal vector of the medial surface at each atom in $\hat{\mathbf{M}}$, and $\mathbf{n}^{avg}$ be the Average of these Normal vectors (AoN). Fig. 2.a shows the medial surface of a myopathic LV at three sequential time points along with the normal vectors of atoms in $\hat{\mathbf{M}}$. Since the atoms of a myopathic region construct a patch-shape on LV, the direction of AoN does not change noticeably during one heart cycle (Fig. 2.b).

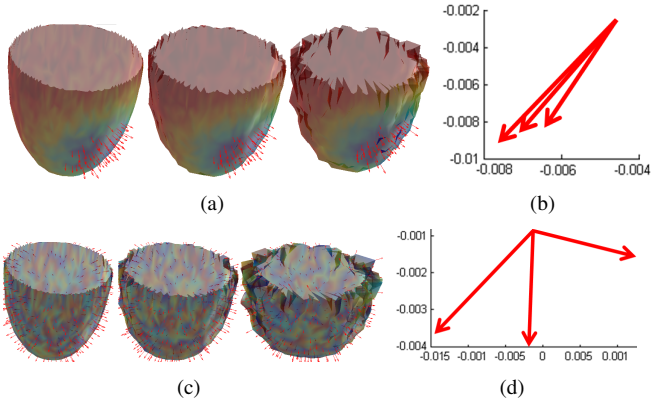

(a) (b) (c) (d)

Fig. 2. The medial surface of (a) a myopathic and (c) a healthy LV at three diastolic time points. Different RWT values are represented with different colors along with the normal vectors of medial surface at atoms in $\hat{\mathbf{M}}$. (b) The Average of the Normal vectors (AoN) of the atoms in $\hat{\mathbf{M}}$ have roughly the same direction at three time points in the myopathic LV, (d) yet AoN of the atoms in $\hat{\mathbf{M}}$ have considerably different directions in a healthy LV.

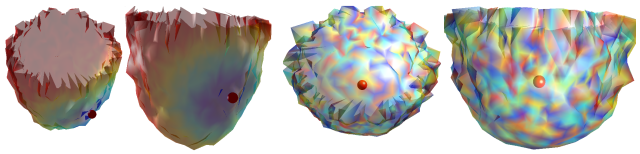

(a) (b)

Fig. 3. (a) MoC of a myopathic LV is located on the medial surface, (b) In a healthy LV, the mean is inside the medial surface.

As aforementioned, some atoms of a healthy LV might belong to $\hat{\mathbf{M}}$, i.e. RWT ≈ 1; however, since there is no myopathic region on a healthy LV, the $\hat{\mathbf{M}}$ atoms in a healthy LV are distributed all over the medial surface and this distribution might change during one heart cycle at sequential time points (Fig. 2.c). As a result, the direction of AoN changes considerably during one heart cycle, and also during different cycles (Fig. 2.d).

2.2. Mean of Centers (MoC)

Let **x** be the center of each atom in $\hat{\mathbf{M}}$ and $\bar{\mathbf{x}}$ be the Mean of the Centers (MoC). In a myopathic LV, the $\hat{\mathbf{M}}$ atoms are concentrated around the myopathic region, thus MoC is close to the medial surface during one heart cycle (Fig. 3.a). In contrast, the $\hat{\mathbf{M}}$ atoms distributed all over the medial surface in a healthy LV, and the corresponding MoC is located inside the medial surface at different time points (Fig. 3.b). Therefore,

we can easily calculate MoC of atoms in $\hat{\mathbf{M}}$ and compare its closeness to the medial surface in different subjects to determine abnormalities.

2.3. The Medial Surface Shape Space

In order to quantify and measure the similarity of the LV deformations reflected by $\hat{\mathbf{M}}$, we embed the deforming shapes into a medial surface shape space, where each point corresponds to a certain LV medial surface. Let $\mathbf{G}$ be the medial surface shape space manifold and $\mathbf{g} \in \mathbf{G}$ be a point corresponding to one medial surface. Based on the shape descriptors and characteristics described in Section 2, we can define the unique shape space as,

$$\mathbf{g} = (\bar{\mathbf{x}}, \hat{r}^{\rho}, \mathbf{n}^{avg}) \in \left\{\mathbb{R}^3 \times \mathbb{R}^+ \times S^2\right\},$$

where $\bar{\mathbf{x}}$ and $\mathbf{n}^{avg}$ are the MoC and AoN of $\hat{\mathbf{M}}$ of $\mathbf{g}$,

$$\hat{r} = \prod_{i \in \hat{\mathbf{M}}} \left(\frac{r_i(t_2)}{r_i(t_1)}\right),$$

is the multiplication of RWT values over all atoms in $\hat{\mathbf{M}}$, and $\rho = \sum_{\hat{\mathbf{M}}} Log_{\mathbf{n}}(\mathbf{S})/|\hat{\mathbf{M}}|$ which measures the average of the log map distance between the normal vector $\mathbf{n}$ and the corresponding spoke vector $\mathbf{S}$ at all the atoms in $\hat{\mathbf{M}}$, which in turn is the geodesic distance between two vectors on sphere S^2.

In our defined medial surface shape space, the geodesic distance connecting two points on the shape space manifold measures the similarity between their corresponding medial surfaces. Let $\mathbf{g}_1 = (\bar{\mathbf{x}}_1, \hat{r}_1^{\rho}, \mathbf{n}_1^{avg})$ and $\mathbf{g}_2 = (\bar{\mathbf{x}}_2, \hat{r}_2^{\rho}, \mathbf{n}_2^{avg})$ be two medial surfaces in $\mathbf{G}$. We project the non-linear shape space onto the linear tangent space using the log map which preserves the geodesic distance, *i.e.*, $d_g(\mathbf{g}_1, \mathbf{g}_2) = \left\|Log_{\mathbf{g}_1}(\mathbf{g}_2)\right\|$, where d_g is the geodesic distance between g_1 and g_2 on the shape space manifold and $Log_{\mathbf{g}_1}(\mathbf{g}_2)$ is their log map. The magnitude of the log map is defined using the linear Euclidean distance measure as,

$$\begin{aligned}\left\|Log_{\mathbf{g}_1}(\mathbf{g}_2)\right\| \quad = \quad & \Big[\left\|\bar{\mathbf{x}}_2 - \bar{\mathbf{x}}_1\right\|^2 + \left\|log(\hat{r}_2^{\rho_2}) - log(\hat{r}_1^{\rho_1})\right\|^2 \\ & + \left\|Log_{\mathbf{n}_1^{avg}}(\mathbf{n}_2^{avg})\right\|^2\Big]^{\frac{1}{2}}, \end{aligned} \tag{2}$$

where $Log_{\mathbf{n}_1^{avg}}(\mathbf{n}_2^{avg})$ is the log map between $\mathbf{n}_1^{avg}$ and $\mathbf{n}_2^{avg}$ on sphere S^2 (Eq. 1).

2.4. Deformation Classification

Let $\mathbf{g}_1, ..., \mathbf{g}_n$ be n points on shape space corresponding to n poses of the LV during one heart cycle. As mentioned in Sections 2.1 and 2.2, the variations of AoN and MoC of a myopathic LV is smaller than those of a healthy LV. As a result, the points $\mathbf{g}_i$ are closer to each other in a myopathic LV than in a healthy LV. Therefore, the variance of the points which reveals the closeness of the points $\mathbf{g}_i$, can be used to classify healthy and myopathic LV's.

Since the points $\mathbf{g}_i$'s are located on a non-linear shape space manifold, we calculate the *intrinsic variance* of $\mathbf{g}_i$'s for each LV rather than the ordinary variance. First, the *intrinsic mean* of the points $\mathbf{g}_i$'s is computed based on the proposed metric as in [8]. Next, the intrinsic variance σ^2 is calculated as,

$$\sigma^2 = \Sigma_{i=1}^n d_g^2(\mu, \mathbf{g}_i)/n = \Sigma_{i=1}^n \left\|Log_{\mu}(\mathbf{g}_i)\right\|^2/n,$$

where μ is the intrinsic mean of $\mathbf{g}_i$'s, and $\|Log_{\mu}(\mathbf{g}_i)\|$ is the geodesic distance between μ and $\mathbf{g}_i$ based on the proposed metric.

3. RESULTS

Five myopathic subjects whose cardiac abnormalities were verified by cardiologists, and nine control subjects participated in this study. CT scans of the heart during one heart cycle were acquired from the subjects with voxel size of $0.5 \times 0.5 \times 0.5\text{mm}^3$, tube voltage of 125kV, FOV=500mm, and gantry angle $0 \sim 15^{\circ}$. Each dataset contains eight time points during one heart cycle.

First, the medial surfaces of different poses are extracted and registered using the method in [5] such that each medial surface contains 400 atoms. Then, the location of each pose embedded in the medial surface shape space is calculated along with the intrinsic variance for each subject. Table 1 illustrates the sensitivity and specificity of our method. The method shows better performance compared with other methods based on the LV cavity, mean radial displacement and mean radial velocity [9]. Indeed, this indicator is very sensitive in detecting myopathic regions.

To better perceive dis/similarity of the deformations, the corresponding medial surface points on the shape space manifold are projected on a 2D plane using the MultiDimensional Scaling method (MDS) and based on the proposed metric. For better visualization, Fig. 4 only illustrates the points corresponding to two myopathic subjects and two healthy subjects after projection on the 2D plane. In the myopathic subjects, since MoC's and AoN's do not change in sequential poses, their corresponding embedded points are located close to each other on the shape space manifold, so are their corresponding points on the 2D plane after the MDS projection(Fig. 4).

Table 1. Sensitivity and Specificity of our method

	Sensitivity	Specificity
Our Method	80.0%	77.8%
Mean Systolic Radial	79.4%	54.9%
Mean Radial Displacement	76.2%	70.9%

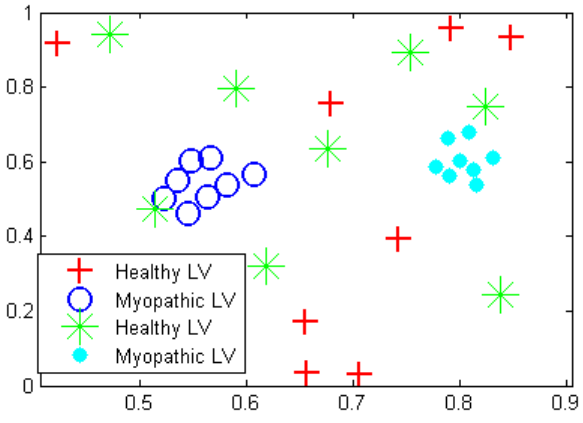

Fig. 4. The projection of two healthy and two myopathic LV motions (each containing 8 motion snapshots) onto the 2D plane illustrates that the points corresponding to the healthy LV are scattered all over the 2D plane, but those of the myopathic LV are concentrated on the same part of the 2D plane.

Table 2. Performance of the algorithm against noisy datasets with different percentages of additive noise variance

Additive Medial Surface Noise	Uniform Noise	Gaussian Noise
1%	88.6%	85.7%
2.5%	83.3%	82.0%
5%	77.0%	78.9%

Due to inaccuracy in the medial surface extraction and also due to existence of noise in the acquired images, the medial surface may not be extract accurately. To evaluate the performance of the method against these inaccuracies, uniform and Gaussian noises are added to the atoms extracted from the healthy and myopathic subjects. The noise was first added to the atom centers ($\mathbf{x}$), i.e. medial surface, and then to the atom radii (r), i.e. wall thickness. The result of the classification is illustrated in Table 2 with different noise distributions. As seen, the performance is acceptable up to 5% of additive noise.

4. CONCLUSIONS

The medial surface shape space is presented to classify and compare LV deformations based on the changes of the wall thickness. Indeed, it is of great use to diagnose the myopathic left ventricles in which myopathic regions do not work normally and the wall thickness is affected accordingly. In particular, we employ RWT values of each LV to detect the candidate myopathic locations. To improve the performance of the RWT values, two shape descriptors AoN and MoC are introduced to construct a non-linear shape space which has great potential to capture the non-linearity of the LV deformation for HCM diagnosis, which reduces subjectivity in the LV deformation analysis. The results on real datasets on myopathic/healthy subjects show high resistance against noise and accurate myopathic/healthy LV classification, which is comparable to the previously reported studies.

5. REFERENCES

[1] B.J. Maron et al., "Cardiovascular preparticipation screening of competitive athletes: a statement for health professionals from the sudden death committee (clinical cardiology) and congenital cardiac defects committee (cardiovascular disease in the young), american heart association," *Circulation*, vol. 94, no. 4, pp. 850–856, 1996.

[2] T. Germans et al., "Structural abnormalities of the inferoseptal left ventricular wall detected by cardiac magnetic resonance imaging in carriers of hypertrophic cardiomyopathy mutations," *Journal of the American College of Cardiology*, vol. 48, no. 12, pp. 2518–2523, 2006.

[3] A. Suinesiaputra, , et al., "Automated detection of regional wall motion abnormalities based on a statistical model applied to multislice short-axis cardiac mr images," *Medical Imaging, IEEE Transactions on*, vol. 28, no. 4, pp. 595–607, 2009.

[4] K. Leung and J. Bosch, "Localized shape variations for classifying wall motion in echocardiograms," *Medical Image Computing and Computer-Assisted Intervention–MICCAI 2007*, pp. 52–59, 2007.

[5] H. Sun et al., "Cardiac medial modeling and time-course heart wall thickness analysis," *Medical Image Computing and Computer-Assisted Intervention–MICCAI 2008*, pp. 766–773, 2008.

[6] S.M. Pizer et al., "Multiscale medial loci and their properties," *International Journal of Computer Vision*, vol. 55, no. 2, pp. 155–179, 2003.

[7] P.A. Yushkevich, "Continuous medial representation of brain structures using the biharmonic pde," *NeuroImage*, vol. 45, no. 1 Suppl, pp. S99, 2009.

[8] P.T. Fletcher, S.M. Pizer, and S.C. Joshi, "Shape variation of medial axis representations via principal geodesic analysis on symmetric spaces," *Statistics and Analysis of Shapes*, pp. 29–59, 2006.

[9] M. Qazi et al., "Automated heart abnormality detection using sparse linear classifiers," *Engineering in Medicine and Biology Magazine, IEEE*, vol. 26, no. 2, pp. 56–63, 2007.